Magnetic frustration in low-dimensional substructures of hulsite $Ni_{5.15}Sn_{0.85}(O_2BO_3)_2$

C. P. C. Medrano,[1,2] D. C. Freitas,[1] E. C. Passamani,[3] J. A. L. C. Resende,[4] M. Alzamora,[5] E. Granado,[6] C. W. Galdino,[6] E. Baggio-Saitovitch,[2] M. A. Continentino,[2] and D. R. Sanchez[1]

[1]*Instituto de Física, Universidade Federal Fluminense, Campus da Praia Vermelha, 24210-346 Niterói, Rio de Janeiro, Brazil*
[2]*Centro Brasileiro de Pesquisas Físicas, Rua Dr. Xavier Sigaud, 150 Urca, 22290-180 Rio de Janeiro, Rio de Janeiro, Brazil*
[3]*Departamento de Física, Universidade Federal do Espírito Santo, 29075-910 Vitória, Espírito Santo, Brazil*
[4]*Instituto de Ciências Exatas e da Terra, Campus Universitário do Araguaia, Universidade Federal do Mato Grosso, 78600-000 Barra do Garças, Mato Grosso, Brazil*
[5]*Campus Duque de Caxias, Universidade Federal do Rio de Janeiro, 25265-008 Rio de Janeiro, Brazil*
[6]*"Gleb Wataghin" Institute of Physics, University of Campinas–UNICAMP Campinas, 13083-859 São Paulo, São Paulo, Brazil*

(Received 3 November 2017; revised manuscript received 20 June 2018; published 31 August 2018)

This paper presents an extensive study of the structural, magnetic, and thermodynamic properties of the hulsite $Ni_{5.15}Sn_{0.85}(O_2BO_3)_2$. The crystal structure of the hulsite has two planar substructures formed by Ni and Sn atoms: one with rectangular configuration and the other with a triangular arrangement. These substructures are linked by the boron ions and by Ni in another site closer to the rectangular arrangement, resulting in a quasi-two-dimensional character. Thus, this system literally adds a new dimension to the study of oxyborates. Our results point to a complex magnetic behavior consistent with these substructures. The planes with rectangular arrangement form a complex magnetic ordering at 180 K (one of the highest magnetic transitions among the oxyborates). The other subsystem, formed by Ni atoms located in a two-dimensional triangular lattice, does not order down to temperatures as low as 3 K. The experimental results suggest a spin-liquid behavior for this subsystem. The magnetic moments of the ions between these planes also freeze at low temperatures. The two magnetic planes coexist as independent subsystems down to the lowest temperatures of our experiments.

DOI: 10.1103/PhysRevB.98.054435

I. INTRODUCTION

Reduced dimensionality and geometrical frustration have attracted considerable interest due to the possible emergence of novel low-temperature magnetic phenomena and spin disordered states, such as spin liquids and spin glass states. Magnetic oxyborates usually with warwickite and ludwigite structures are known to present unconventional magnetic properties. These properties are related to the presence of low-dimensional substructures, in the form of ladders in ludwigites and ribbons in warwickites. For instance, charge ordering transition are observed in ludwigite $Fe_3O_2BO_3$ [1–3] and warwickite Fe_2OBO_3 [1,4], while there is no evidence of charge ordering in their homometalic counterparts ludwigite $Co_3O_2BO_3$ [3,5] and warwickite Mn_2OBO_3 [6]. In addition, partial magnetic order was found in ludwigites that contain Fe^{3+} ions like $Fe_3O_2BO_3$ [1–3], $Co_2FeO_2BO_3$ [3,7], and $Ni_2FeO_2BO_3$ [8]. Due to frustration and disorder, spin glass behavior is usual in the ludwigites containing nonmagnetic ions, such as $Co_5Ti(O_2BO_3)_2$ [9] and $Ni_5Ge(O_2BO_3)_2$ [10], and in the warwickites $MgFeBO_4$ and $CoFeBO_4$ [11,12]. Also a spin liquid–random singlet phase was found in disordered warwickite $MgTiOBO_3$ [13].

Magnetic oxyborates with hulsite structure are much less explored. They are known to have a strong two-dimensional (2D) character related to planar substructures. Hulsite crystallizes in space group $P2/m$ and has the general formula $M_{6-x}M'_x(O_2BO_3)_2$, where M is a divalent or trivalent metal ion and M' is a tetravalent or pentavalent metal ion. The metal ions occupy five nonequivalent crystallographic sites in oxygen octahedral coordination. Four sites form two families of parallel sheets and the fifth site is in between those sheets. Hulsite can be found in nature with an iron-based chemical composition but, up to now, only two hulsites have been synthesized, $Ni_{5.33}Sb_{0.67}(O_2BO_3)_2$ [14] and $Co_{5.52}Sb_{0.48}(O_2BO_3)_2$ [15]. They have similar structure parameters and the same nonmagnetic ion Sb^{5+}, occupying only one site (site 1). Concerning the magnetic properties, only dc susceptibility is available for $Ni_{5.33}Sb_{0.67}(O_2BO_3)_2$, and the authors described the results as a possible partial magnetic ordering at ∼170 K and an antiferromagnetic (AFM) ordering increasing below 40 K [14]. In $Co_{5.52}Sb_{0.48}(O_2BO_3)_2$, on the other hand, the whole structure orders magnetically below 42 K, with an antiferromagnetic type structure. Specific heat measurements at low temperatures show a dominant gapped T^2 contribution that has been attributed to magnons with a linear dispersion relation propagating in planes [15]. These results give evidence of the two-dimensional nature of the magnetic ordering in this system [15].

In this paper, we combine macroscopic and local information to study the hulsite $Ni_{5.15}Sn_{0.85}(O_2BO_3)_2$. Similar to the hulsites already known, it contains a nonmagnetic ion (Sn) that happens to be a Mössbauer probe. Thus, the application of Mössbauer spectroscopy technique, which has already been shown to be a very useful tool in the study of magnetism of oxyborates [16–18], will give local information on the magnetic properties of this compound. This information is unique since it cannot be obtained with conventional techniques, such as magnetization, specific heat, and resistivity. In hulsite

$Ni_{5.15}Sn_{0.85}(O_2BO_3)_2$, most of the Ni ions have an oxidation state 2+ with a spin $S = 1$, as in $Ni_{5.33}Sb_{0.67}(O_2BO_3)_2$. The dc susceptibility of these two Ni hulsites is very similar. The present study indicates that the planar substructures have different magnetic behavior, related to disorder and magnetic frustration. A spin glass like transition of the subsystem formed by Ni ions located in a plane with a rectangular arrangement occurs at 180 K, whereas Ni ions located in planes with a triangular arrangement do not order down to 3 K. The existence of these planes with strong frustrated interactions makes this material compatible with other Ni systems such as $Ba_3NiSb_2O_9$-6H-B [19,20] and $NiGa_2S_4$ [21], which are strong candidates to be in a spin liquid state. The low-temperature magnetic and thermodynamic properties of hulsite $Ni_{5.15}Sn_{0.85}(O_2BO_3)_2$ studied here suggest that a spin liquid state could be formed in the plane with triangular arrangements of this material. Indeed, the low-temperature specific heat of this hulsite has a linear temperature term of the order (see below) observed in another spin-1 quantum spin liquid (QSL) candidate, $Ba_3NiSb_2O_9$-6H-B [19,20]. We must note that our compound is different from the QSL candidates mentioned above because it has site occupancy disorder. However, in a recent work, the disordered double perovskite $Sr_2Cu(Te_{0.5}W_{0.5})O_6$ has shown spin liquid like behavior [22]. In this context, our results can contribute to the understanding of the role of disorder in highly frustrated magnetic systems.

II. EXPERIMENT

A. Synthesis

The crystals were synthesized at UFF from a 5 : 1 : 2 molar mixture of NiO_2 : SnO_2 : H_3BO_3 with a large excess of borax. The mixture was heated at 1160 °C for 30 minutes and cooled down to 600 °C in 24 hours. Then, the oven was turned off. The bath was dissolved in hot water and the crystals washed in diluted hydrochloric acid. Planar shaped black crystals up to 2 mm length were obtained. The purity of the sample was confirmed by x-ray powder and single-crystal diffraction.

B. Structural characterization

A planar shaped twin crystal was employed for data collection from x-ray diffraction (XRD). The measurement was carried out on a D8 Venture Bruker diffractometer at room temperature, using Incoatec Microfocus Source (IμS) x-ray, Mo $K\alpha$ radiation. The crystal was mounted on a Kappa goniometer, and the data were collected using a PHOTON 100 detector. Data collection was performed with APEX2 v4.2.2 [23]. CELL_NOW [24] was used for indexing two twin components generating a ".p4p" file for integration. Data integration was carried out using SAINT [25]. Empirical numerical absorption correction was performed with the TWINABS program [26]. The structure was refined as a two-component twin [BASF = 0.494(3)]. For twinned crystals, the batch scale factor (BASF) specifies the fractional contributions of the various twin components. The full-matrix least-squares refinements based on F^2 with anisotropic thermal parameters were carried out using SHELXL-2013 [27] program packages with WINGX [28] and SHELXLE [29] software interfaces.

TABLE I. Crystal data and structure refinement of $Ni_{5.15}Sn_{0.85}(O_2BO_3)_2$.

Empirical formula from x-ray analysis	$Ni_{5.15(2)}Sn_{0.85(2)}B_2O_{10}$
Formula weight	585.16 g/mol
Wavelength	0.71073 Å
Crystal size	$0.061 \times 0.058 \times 0.029$ mm^3
Temperature	295 K
Crystal system	monoclinic
Space group	(No. 10) $P2/m$
Unit cell dimension $a =$	5.4185(7) Å
$b =$	3.0504(4) Å
$c =$	10.6122(13) Å
$\beta =$	94.707(4)°
Volume	174.81(4) Å^3
Z	1
Density (calculated)	5.558 Mg/m^3
Absorption coefficient	16.632/mm
$F(000)$	277
θ range (degrees)	3.773 to 32.314
Index range $h =$	−8, 8
$k =$	0, 4
$l =$	0, 15
Reflections collected/unique	7672/716
Independent reflections	716
Completeness to $\theta = 32.314$	97.9 %
Refinement method: full-matrix least squares on F^2	
Data/restraints/parameters	716 / 12 / 63
Goodness-of-fit on F^2	1.109
Final R indices $[I > 2\sigma(I)]$	R1 = 0.0375, wR2 = 0.0917
R indices (all data)	R1 = 0.0407, wR2 = 0.0935
Largest diff. peak and hole	3.496 and −2.650 e Å^{-3}

Crystallographic tables were generated by WINGX [28]. Crystal data, data-collection parameters, and structure-refinement data are displayed in Table I.

Figure 1(a) shows the whole structure projected along the c axis. The unitary cell, represented by a continuous line, is composed by five metal sites within oxygen octahedra and boron in a triangular oxygen coordination. Sites 1, 2, and 3 are randomly occupied by Ni and Sn atoms, while sites 4 and 5 are exclusively occupied by Ni atoms, see Fig. 1 and Table II. There is no homometallic hulsite, and the random presence of Sn atoms at sites 1, 2, and 3 produces a site occupancy disorder in this material.

The main bond lengths in this compound are shown in Table III. It is worth noting that the shortest intermetallic distance is between ions at sites 2 and 3 ($d_{2\text{-}3} = 2.7093$ Å). A scheme of the planar substructures formed by Ni and Sn metal atoms is presented in Fig. 1(b), where, for simplicity, boron and oxygen atoms are omitted. The colored lines shows the nearest-neighbor distances. One planar substructure is formed by metal sites 2 and 3 in a rectangular arrangement (blue), the other substructure is formed by sites 1 and 4 in a triangular arrangement (pink). In the following, we will refer to these substructures as 2-3 and 1-4 *layers* respectively. Thus, the hulsite can be viewed as a layered material with

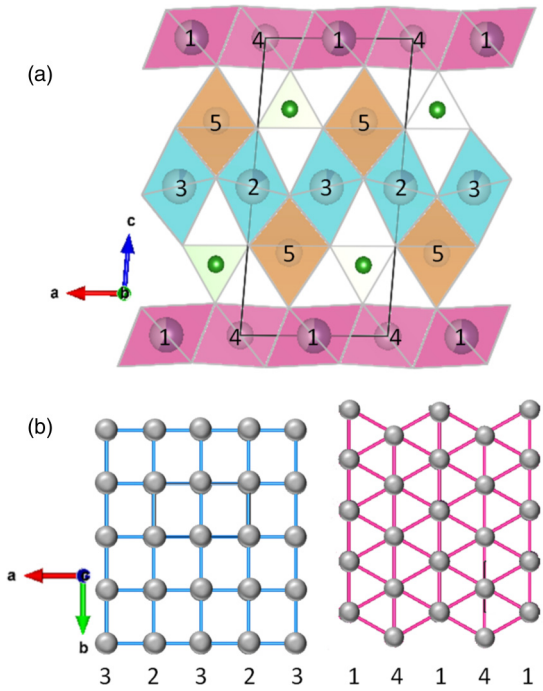

FIG. 1. Schematic structure of $Ni_{5.15}Sn_{0.85}(O_2BO_3)_2$. (a) The whole structure formed by five metal sites within oxygen octahedra, indicated by numbers, and boron in a triangular oxygen coordination. The continuous black line indicate the unit cell. Sites 1, 2, and 3 are occupied randomly by Ni and Sn ions, sites 4 and 5 are exclusively occupied by Ni atoms. The structure is projected along the *b* axis. (b) Planar substructures formed by metal ions projected along the *c* axis; here oxygen and boron atoms are omitted.

the bidimensional 2-3 and 1-4 layers (5.0308 Å apart) stacked alternatingly along the -*c* axis. The Ni ions at sites 5 are located between these two layers and are closer to the 2-3 layer.

The bond angles *M*-O-*M*, which are important to discuss superexchange magnetic interactions, are given in Table III. The Ni (Sn) at the 1-4 layer have six and four bond angles of ∼96° and ∼120°, respectively. Analogously, the Ni (Sn) at the 2-3 layer have eight and four bond angles of ∼91° and 162°, respectively. Finally, the Ni at site 5 have four and three bond angles of ∼98° and ∼120°, respectively. The smaller (larger) angles correspond to the nearest neighbor (next-nearest neighbor) Ni (Sn) ions.

So, the hulsite contains 86% Ni atoms and 14% Sn. Of all the Sn ions, 31% of them are located in the 2-3 layer, occupying arbitrarily sites 2 and 3, and the remaining 69% of Sn ions lie in the 1-4 layer occupying (randomly) only site 1.

C. XAS spectroscopy

The room-temperature Ni *K*-edge XAS spectrum of $Ni_{5.15}Sn_{0.85}(O_2BO_3)_2$ was collected under the transmission mode at the XAFS2 beamline of the Brazilian Synchrotron Laboratory (LNLS). The normalization of the spectra was done through standard procedures using the software ATHENA [31] and the fitting of the experimental data was performed using a Python script based on the nonlinear least squares method.

TABLE II. Fractional coordinates, site occupancy factor (SOF), the occupation (Occ.) of atoms per site normalized by the SOF factor, and equivalent isotropic displacement parameters ($Å^2 \times 10^3$) for $Ni_{5.15}Sn_{0.85}(O_2BO_3)_2$. The SOF values must be multiplied by the factor 4 in order to obtain the number of atoms in the unit cell. U(eq) is defined as one third of the trace of the orthogonalized U_{ij} tensor [30].

Site	x/a	y/b	z/c	SOF	Occ.	U(eq)
Ni1	0.5	1	1	0.103	0.411	6(1)
Sn1	0.5	1	1	0.147	0.589	6(1)
Ni2	0	0	0.5	0.206	0.824	5(1)
Sn2	0	0	0.5	0.044	0.176	5(1)
Ni3	0.5	0	0.5	0.228	0.910	4(1)
Sn3	0.5	0	0.5	0.022	0.090	4(1)
Ni4	0	0.5	1	0.25	1	5(1)
Ni5	0.2835(2)	0.5	0.72130(9)	0.5	1	5(1)
B	0.2057(14)	0	0.2384(9)	0.5	1	1(1)
O1	0.2539(10)	0.5	0.5298(6)	0.5	1	5(1)
O2	0.3127(11)	0.5	0.9068(5)	0.5	1	5(1)
O3	−0.0067(11)	0	0.3020(6)	0.5	1	5(1)
O4	0.8116(12)	1	0.8928(6)	0.5	1	6(1)
O5	0.4421(11)	0	0.3016(6)	0.5	1	7(1)

Experimental errors of fitted quantities are statistical only and represent one standard deviation.

Figure 2(a) shows the normalized Ni *K*-edge absorption spectra of $Ni_{5.15}Sn_{0.85}(O_2BO_3)_2$ and NiO. A fitting for $Ni_{5.15}Sn_{0.85}(O_2BO_3)_2$ was performed using a model with five Gaussian peaks, denoted by letters *a* to *e*, added to an arctan function with a linear background representing the edge step (*f*). The inset at the right of Fig. 2(a) shows a Gaussian function together with its first (blue curve) and second (red curve) derivatives. Feature *a* is the pre-edge peak, associated with empty 3*d* states. Features *b* and *c* are dipolar transitions to empty 4*p* states. Peak *c*, whose area was fixed at 5% of the area of the main peak *b* to minimize correlation between fitting parameters, is blueshifted by 1.65(20) eV with respect to feature *b*. An alternative fitting model with four Gaussian peaks (i.e., excluding feature *c*), also gives a satisfactory fitting of the absorption spectrum [see blue dashed line in Fig. 2(a)]. Features *d* and *e* are possibly related to multiple

TABLE III. Selected bond lengths *M*–*M* in Å and bond angles *M*–O–*M* in degrees for $Ni_{5.15}Sn_{0.85}(O_2BO_3)_2$. The average Ni–O distance is 2.087 Å.

Ni1–Ni4	3.1091(3)	Ni2–Ni3	2.7093(4)
Ni1–Ni5	3.4468(9)	Ni4–Ni5	3.4428(4)
Ni2–Ni5	3.0999(3)	Ni3–Ni5	3.1097(9)
Ni1–O2–Ni1	96.6(3)	Ni1–O4–Ni4	94.8(3)
Ni1–O2–Ni4	99.5(3)	Ni1–O2–Ni5	118.8(3)
Ni2–O1–Ni2	95.5(3)	Ni2–O1–Ni3[b]	162.4(3)
Ni2–O1–Ni3[a]	82.03(4)	Ni2–O1–Ni5	98.68(17)
Ni2–O3–Ni5	94.02(17)	Ni3–O1–Ni3	95.1(3)
Ni3–O1–Ni5	98.89(17)	Ni3–O5–Ni5	93.74(17)
Ni4–O4–Ni4	92.3(3)	Ni4–O2–Ni5	119.1(3)

[a]Nearest neighbor.
[b]Next-nearest neighbor.

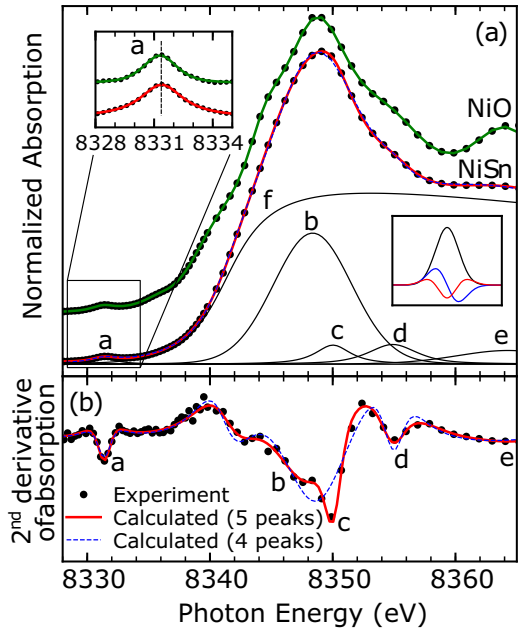

FIG. 2. (a) Ni K-edge XAS absorption spectrum of $Ni_{5.15}Sn_{0.85}(O_2BO_3)_2$ and the reference compound NiO. Black symbols show the experimental data while the red solid line represents a fitted curve for $Ni_{5.15}Sn_{0.85}(O_2BO_3)_2$ (see text). The green solid line is a fit for NiO using seven Gaussian peaks. (b) Second derivative of the experimental (symbols) and fitted absorption spectra of $Ni_{5.15}Sn_{0.85}(O_2BO_3)_2$.

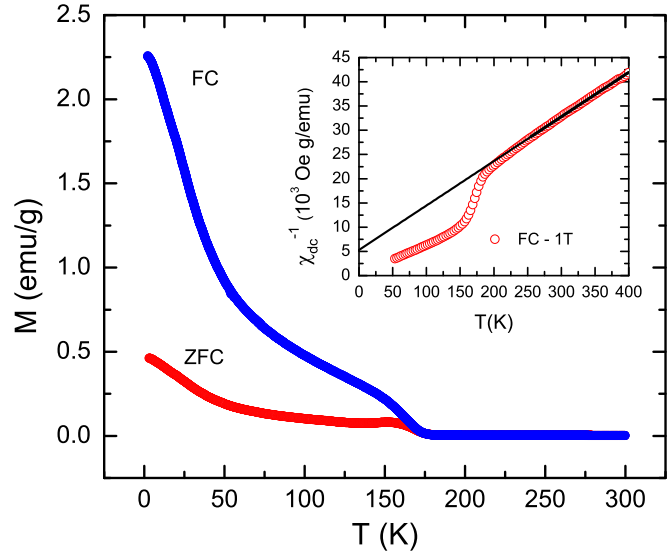

FIG. 3. Magnetization versus temperature for $Ni_{5.15}Sn_{0.85}(O_2BO_3)_2$ under an applied magnetic field of 100 Oe. Inset: Inverse magnetization in a 1-T magnetic field.

scattering effects and backscattering from neighboring ions, in analogy with Co oxides [32]. The inset by the left corner of Fig. 2(a) shows the pre-edge peaks for $Ni_{5.15}Sn_{0.85}(O_2BO_3)_2$ and NiO after background substraction. The centers of the pre-edge peak in both compounds lie at the same energy [8331.38(3) and 8331.33(4) eV for $Ni_{5.15}Sn_{0.85}(O_2BO_3)_2$ and NiO, respectively]. Also, the central positions of the main peak b are the same for both oxides 8348.8(4) eV for NiO and 8348.4(1) eV for $Ni_{5.15}Sn_{0.85}(O_2BO_3)_2$. Notice that the energy positions of the pre-edge and main peaks are indicators of the average oxidation state of Ni, blue shifting by ∼0.5 and 1.5 eV, respectively, under $Ni^{2+} \rightarrow Ni^{3+}$ oxidation [33–38]. Thus, our observations for $Ni_{5.15}Sn_{0.85}(O_2BO_3)_2$ in comparison to NiO indicate that the Ni valence in $Ni_{5.15}Sn_{0.85}(O_2BO_3)_2$ is predominantly +2, as expected.

The charge neutrality condition in $Ni_{5.15}Sn_{0.85}(O_2BO_3)_2$ suggests the possibility of a small (∼5%) level of Ni^{3+}, which is verified by a careful Ni K-edge XAS spectral shape analysis. Figure 2(b) shows the second derivative of the spectrum of $Ni_{5.15}Sn_{0.85}(O_2BO_3)_2$ together with the second derivative of the fitting curves for the four-peak and five-peak models introduced in Fig. 2(a). While feature c is not essential for the good fitting of the direct XAS spectrum given in Fig. 2(a), its presence is necessary to fit appropriately the second-derivative curve shown in Fig. 2(b). Since the position of peak c is ∼1.5 eV above feature b, peak c may be associated with the main peak of a small fraction (∼5%) of Ni ions with valence +3, as expected. While the presence of peak c in the Ni K edge absorption spectrum of $Ni_{5.15}Sn_{0.85}(O_2BO_3)_2$ is consistent with the presence of a small fraction of Ni^{3+} in the structure, alternative interpretations are also possible. For instance, peak c might be a spectral feature ascribed to a fraction of Ni^{2+} ions that is specifically located in one of the five possible Ni sites of the hulsite structure.

D. Magnetic measurements

The magnetic measurements were performed on powdered-single crystals of hulsite $Ni_{5.15}Sn_{0.85}(O_2BO_3)_2$ using a commercial Quantum Design physical property measurement system (PPMS) at Universidade Federal do Espírito Santo.

Figure 3 shows the temperature dependence of magnetization curves for field-cooled (FC) and zero-field-cooled (ZFC) procedures, with applied magnetic fields of 100 Oe. In both cases, lowering the temperature down to 2 K, the magnetization increases without reaching a maximum. The magnetization rises sharply at ∼180 K and for lowest temperatures the ZFC and FC curves diverge. This temperature coincides with the beginning of the magnetic broadening of the Mössbauer spectra, to be shown later, so we can attribute this change in the magnetization to the onset of the magnetic transition. In the derivative of the magnetization, subtle changes occur at low temperatures as a maximum close to $T \sim 20$ K. Above the magnetic transition, the magnetization decreases asymptotically with increasing the temperature and can be described by the Curie-Weiss law. The linear fit of the 1-T FC curve (see inset) leads to a Curie constant $C = 10.90 \times 10^{-3}$ emu K $g^{-1}Oe^{-1}$ with a Curie-Weiss temperature $\theta_{CW} = -57.8$ K, indicating the predominance of antiferromagnetic interactions. From the Curie constant, we determine the effective moment $p_{eff} = 7.15\mu_B$ per formula unit (f.u.).

Information on the spin state of Ni ions can be obtained by considering that the Sn atoms have oxidation state 4+ (as shown by Mössbauer spectroscopy data); then charge balance on $Ni_{5.15}Sn_{0.85}(O_2BO_3)_2$ leaves 4.89 atoms of Ni^{2+} and 0.26 atoms of Ni^{3+} per f.u. If we consider that all the Ni atoms are in the high spin (HS) state, the spin only moment

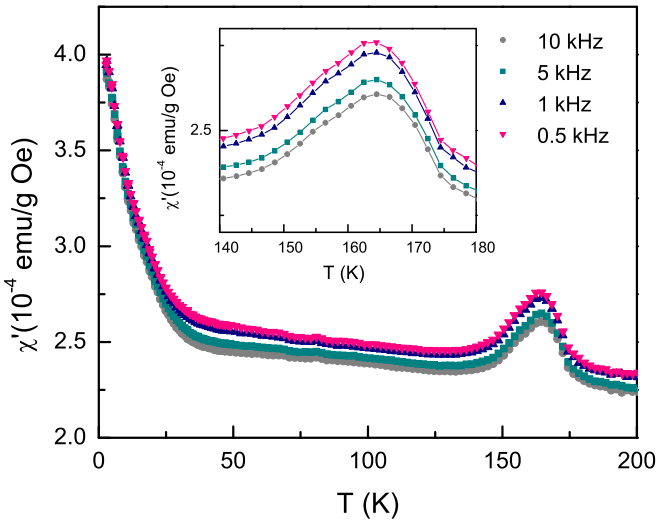

FIG. 4. Real part of the ac susceptibility for $Ni_{5.15}Sn_{0.85}(O_2BO_3)_2$ as a functions of temperature for 0.5, 1, 5, and 10 kHz.

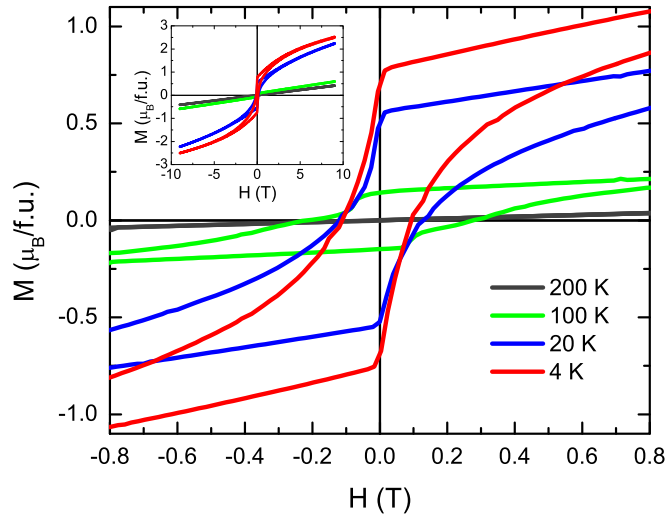

FIG. 5. $Ni_{5.15}Sn_{0.85}(O_2BO_3)_2$ magnetization versus small applied magnetic field curves at 4, 20, 100, and 200 K.

per f.u. could be calculated as $p_{\text{eff}} = \sqrt{p_1^2 + p_2^2 + p_3^2 + \cdots}$, used for systems with two or more different magnetic ions [39,40]. For $Ni_{5.15}Sn_{0.85}(O_2BO_3)_2$ the value of $p_{\text{eff}} = \sqrt{4.89(2.83)^2 + 0.26(3.87)^2} = 6.56\mu_B/(\text{f.u.})$. Then, the effective experimental moment is consistent with the expected value.

Figure 4 displays the real part of the ac susceptibility (χ') for different frequencies as a function of temperature. When lowering the temperature, the susceptibility first increases gradually. Between 180 and 130 K a peak is observed with a maximum value at ∼164 K. The position of the maximum is slightly shifted to higher temperatures as the frequency is increased (there is a shift smaller than ∼0.5 K for two decades in frequency; see inset of Fig. 4) and could be related with disorder or spin glass state [41]. For temperatures lower than 130 K, the susceptibility increases again and at ∼25 K a second drastic rise is observed, but this time without reaching a saturation down to 3 K, the lowest temperature of the experiment.

Figure 5 presents the magnetization curves as a function of applied magnetic fields for different temperatures. Below 180 K, hysteresis consistent with a spin glass phase is observed. At 150 K the hysteresis loop is symmetric, with a coercive field of 540 Oe and a remanent magnetization of $6.2 \times 10^{-2}\mu_B/(\text{f.u.})$.

E. Mössbauer spectroscopy

The hulsite $Ni_{5.15}Sn_{0.85}(O_2BO_3)_2$ ^{119}Sn Mössbauer spectra were taken with natural abundance of ^{119}Sn isotope of 8.6%. The sample was installed at Centro Brasileiro de Pesquisas Físicas (CBPF) in a Montana variable temperature closed-cycle cryostat in the range temperature from 3 to 300 K. The $^{119m}Sn : CaSnO_3$ source was kept at room temperature, moving in a sinusoidal mode outside of the cryostat. The ^{119}Sn Mössbauer spectra for different temperatures are shown in Fig. 6.

The room temperature spectrum shows a unique paramagnetic doublet with quadrupole splitting $\Delta E_Q = 1.12(1)$ mm/s, isomer shift $\delta = 0.21(1)$ mm/s (relative to $BaSnO_3$ at room temperature), and linewidth $\Gamma = 0.98(3)$ mm/s. The isomer shift value is characteristic of a Sn^{4+} oxidation state [42]. The observed linewidth is somewhat larger than 0.85 mm/s found for the related $Co_5Sn(O_2BO_3)_2$ ludwigite, where the Sn atoms occupy a unique site with an octahedral oxygen coordination [18]. The increase of the linewidth can be explained if we consider that Sn ions in $Ni_{5.15}Sn_{0.85}(O_2BO_3)_2$ randomly occupy three sites (1, 2, and 3), giving rise to small variations in quadrupole splitting. The presence of SnO_2 impurity in the sample was precluded since its corresponding Mössbauer spectrum, although it is also a doublet, has hyperfine parameters different from those observed here [42].

The Mössbauer spectra between 300 and 180 K were fitted with a unique doublet, with a slightly increased linewidth. Below ∼180 K, magnetic hyperfine splitting is observed in Mössbuer spectra owing to the Zeeman interaction of the Sn nuclei with the effective hyperfine magnetic field B_{hf}; see Fig. 6. We want to mention at this point that, as Sn atoms carry no local magnetic moment, the B_{hf} at the Sn nuclei develops because of the transfer of spin density from the magnetic Ni^{2+} to the diamagnetic Sn^{4+} ion [43]. The transfer occurs through the direct Ni-Sn and indirect Ni-O-Sn exchange interactions. The contribution of the indirect exchange interaction to the B_{hf} is referred to as the supertransferred hyperfine magnetic field ($B_{\text{hf}}^{\text{st}}$), and for the case of a Sn ion with an outer 5s shell in a matrix containing magnetic cations bonded through oxygen anions it has the following expression [43]:

$$B_{\text{hf}}^{\text{st}} = 525N^4k\left[-\sum_{n=1}^{4} S_{ns}\varphi_{ns}(0) + a_5\varphi_{5s}(0)\right]^2 \times \left(A_\sigma^2 - A_\pi^2\right)\cos^2\vartheta + A_\pi^2, \quad (1)$$

where k is the number of Ni ions surrounding the central Sn, N is a normalization constant, $\varphi_{ns}(0)$ are the s-wave functions of tin, and S_{ns} and a_5 are the overlap and transfer parameters, respectively, for O^{2-}–Sn^{4+}. A_σ^2 and A_π^2 are the covalence parameters of the Ni^{2+}-O^{2-} bond and generally do

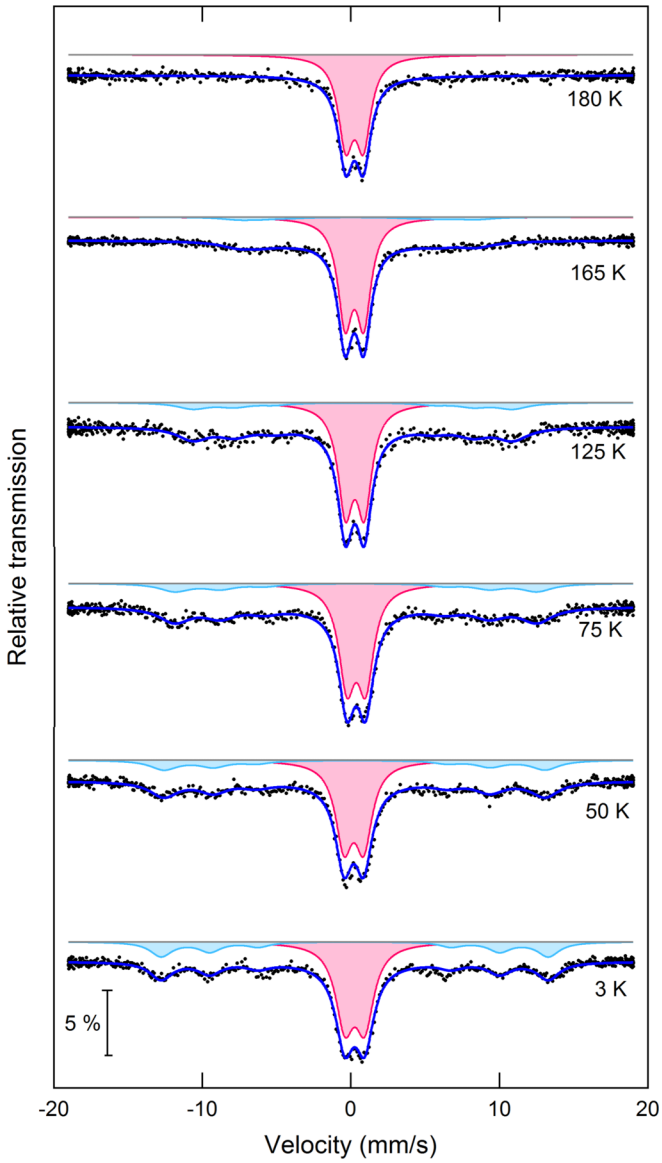

FIG. 6. ^{119}Sn Mössbauer spectra of $Ni_{5.15}Sn_{0.85}(O_2BO_3)_2$ in the temperature range $180 \leqslant T \leqslant 3$ K. For 180 K only one doublet was used to fit the spectra. Below 175 K, all the spectra were fitted with one paramagnetic (pink) and one magnetic (light blue) subspectra.

not depend of the Ni^{2+}-O^{2-} separation, and ϑ is the angle of the Ni-O-Sn exchange bond. Then, the magnitude and direction of the magnetic hyperfine field at the ^{119}Sn nuclei are determined by the resultant of the direct and indirect interactions with magnetic moments of the Ni atoms around them [42,43]. Two subspectra are needed to resolve the spectra below 180 K, one of them corresponding to a paramagnetic doublet and the other to a magnetic sextet.

Linewidth Γ, quadrupole splitting ΔE_Q, isomer shift δ, transferred magnetic hyperfine field B_{hf}, and the angle θ (the angle between the main component of the electric field gradient V_{ZZ} and B_{hf}) were the free fitting parameters. Furthermore, we assumed the quadrupole asymmetry parameter $\eta = 0$ (for an axial symmetry), as it is expected for ^{119}Sn on a regular octahedral site.

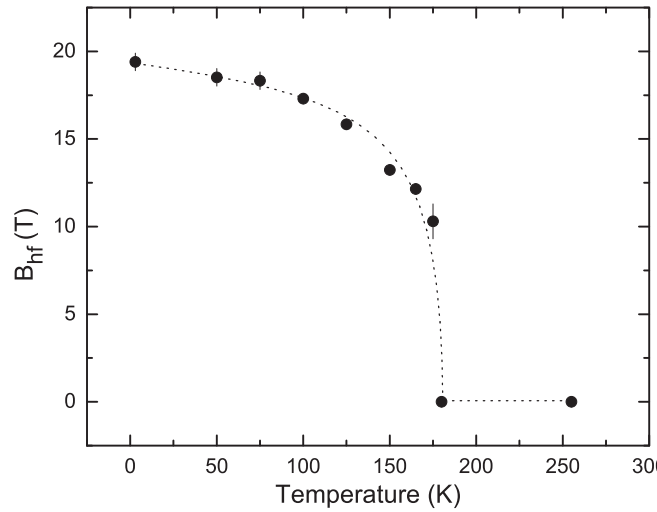

FIG. 7. Temperature dependence of the transferred magnetic hyperfine field (B_{hf}) at Sn nuclei corresponding to the sextet used to fit the spectra of hulsite $Ni_{5.15}Sn_{0.85}(O_2BO_3)_2$.

For all the magnetic subspectra the angle θ is either just the so-called *magic angle* ($\theta \sim 55^\circ$) or is not well defined, i.e., all angles in the range $0 \leqslant \theta \leqslant 90^\circ$ occur with equal probability. One cannot distinguish between these two possibilities; however, the rather broadened magnetic subspectra [$\Gamma(3\text{ K}) = 1.85(6)$ mm/s] make the second possibility more likely. The transferred magnetic hyperfine field B_{hf} increases with decreasing temperature from $B_{hf}(180\text{ K}) \simeq 0$ T to $B_{hf}(3\text{ K}) \simeq 20.1$ T (Fig. 7). The onset of magnetic transition below 180 K is clearly seen. At 3 K, the absorption area of the magnetic subspectra reach 37% of the total area and the remaining 63% correspond to the slightly broad paramagnetic doublet. Relating this result with the single-crystal XRD, where it is shown that 69% of the total ions of Sn go to site 1, we attribute the quadrupole doublet observed at low temperatures to Sn ions at site 1, where they do not *feel* a measurable transferred magnetic hyperfine field, even at 3 K. On the other hand, a pronounced line broadening of the doublet was observed as the temperature is reduced below the magnetic transition temperature [from $\Gamma(200\text{ K}) = 1.11$ mm/s to $\Gamma(3\text{ K}) = 1.44$ mm/s]. This line broadening could be related to a slow relaxation of the Ni spins at site 4 surrounding the Sn ion, as will be discussed below.

F. Specific heat measurements

Specific heat measurements as a function of temperature and magnetic field were performed with randomly oriented needle crystals using a commercial Quantum Design Dynacool PPMS at CBPF. Specific heat measurements of $Ni_{5.15}Sn_{0.85}(O_2BO_3)_2$ in the range of temperature $2 \leqslant T \leqslant 200$ K are plotted in Figs. 8 and 9. Cooling the system through the temperature of the maximum in the susceptibility and down to 50 K, the zero-field specific heat shows no obvious sharp features typical of structural or magnetic order. For lower temperatures, a rounded peak with a maximum at 20 K is observed. Its position does not change for applied magnetic fields as high as 9 T; only a slight flattening of the peak is observed at 9 T. The peak

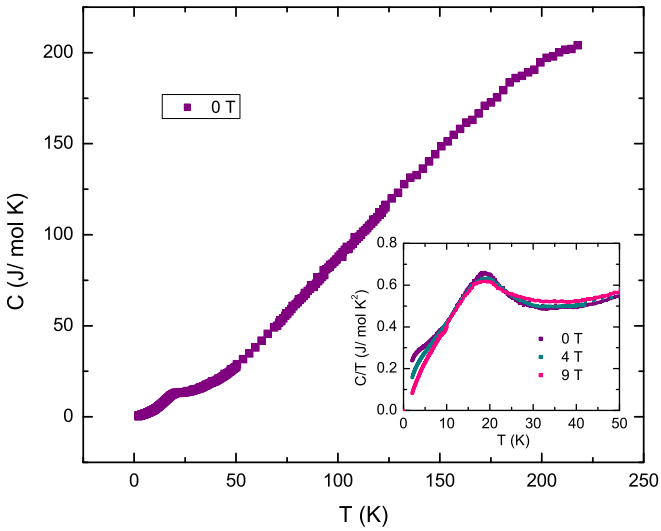

FIG. 8. Hulsite $Ni_{5.15}Sn_{0.85}(O_2BO_3)_2$ specific heat plotted as C vs T for applied magnetic fields of 0, 4, and 9 T. Inset: Low-temperature range plotted as C/T vs T.

observed at 20 K in the specific heat corresponds only to slight changes in the magnetic measurements.

The fitting of the low-temperature specific heat for different magnetic fields is displayed in Fig. 9. In zero field, the specific heat is well fitted by two power laws, linear and square in temperature. This type of behavior has previously been seen in other magnetic oxyborates [15]. The linear term is generally associated with disorder due to the large magnetic frustration present in these systems [9]. The T^2 term is attributed to magnetic elementary excitations with a linear dispersion in a nearly 2D antiferromagnetic system, and has been observed in another Ni-based 2D frustrated magnet [21]. The specific heats in magnetic fields of 4 and 9 T show distinct behavior. They

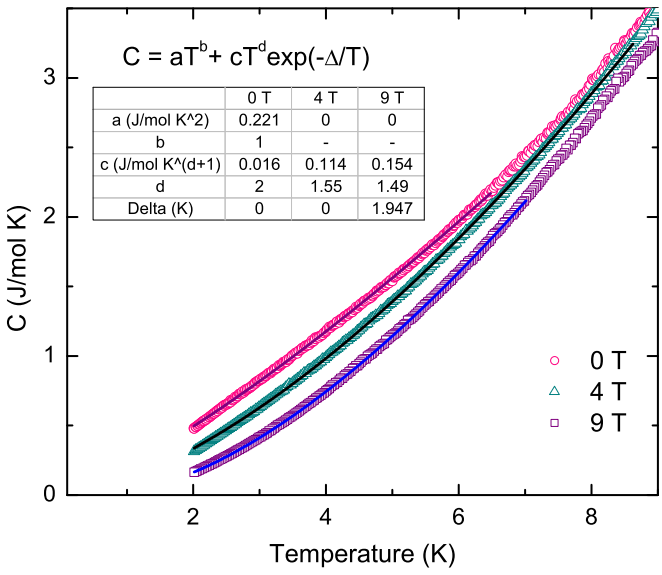

FIG. 9. Low-temperature specific heat of hulsite $Ni_{5.15}Sn_{0.85}(O_2BO_3)_2$ plotted as C vs T for 0 and 9 T. The solid lines are the fits described in the main text.

display a nearly $T^{3/2}$ temperature dependence that suggests the presence of ferromagnetic magnons in a 3D system. The 9-T data require the presence of a spin wave gap, which is not the case for the 4-T results. If the magnetic field, as we suggest, is inducing a phase transition from the antiferromagnet to a fully polarized ferromagnetic system at a critical field H_c, the spin wave gap can be defined as $\Delta_{sw} = g\mu_B S_{eff}(H - H_c)$, where H_c in our system is nearly temperature independent. The simple power-law behavior of the specific heat at 4 T suggests that $H_c \approx 4$ T in our system. Using the experimental gap $\Delta_{sw} \approx 2$ K from the specific heat data at 9 T and $H_c = 4$ T, we obtain an average effective moment $S_{eff} = 0.3$.

III. DISCUSSION

Cooling down the sample below 180 K, a complex ^{119}Sn Mössbauer spectrum, split by magnetic hyperfine interactions appears. 37% of the Sn ions feel a transferred magnetic hyperfine field of $B_{hf} = 19.4$ T from the neighboring Ni magnetic ions, and the remaining fraction (63%) display only a quadrupole splitting. To know the causes of this relatively high B_{hf}, we have to check the direct Sn-Ni and indirect Sn-O-Ni^{2+} bonds that contribute to the B_{hf} at the Sn nuclei. In the 2-3 and 1-4 layers the octahedra of two neighboring Ni (Sn) ions share a common edge, and the electronic configuration of Ni^{2+} $3d^8(t_{2g}^6 e_g^2)$ involves the half-filled e_g orbitals which participate in the Sn-O-Ni^{2+} exchange interaction. The superexchange ferromagnetic 90° couplings are usually weak [44] and consequently small supertransferred hyperfine fields from neighboring Ni ions are expected. In the same way, small values of 120° superexchange integrals found in $Ni_5GeB_2O_{10}$ [10] predict values of supertransferred hyperfine field not too large for a 120° interaction Ni^{2+}-O-Sn^{4+}. Actually, ^{119}Sn Mössbauer spectroscopy studies in Sn:$NiTiO_3$ have shown that (neglecting the contribution from a Ni at 90°) the B_{hf} at Sn nuclei due to three Ni^{2+} cations with the same spin direction along the 130° interaction Ni^{2+}-O-Sn^{4+} bonds is 5.25 T [45] (1.8 T per Ni ion). Smaller values of supertransferred hyperfine field are expected for a $\vartheta = 120°$ interaction bonds, as can be inferred from Eq. (1). On the other hand, the antiferromagnetic 180° superexchange interaction, which is more favorable for transfer of the spin density through e_g-p_σ bonds, is strong and can give rise to large supertransferred B_{hf}. In fact, in the Sn doped antiferromagnetic NiO, the large $B_{hf} = 22.9$ T is created by six next-nearest Ni^{2+} ions with the same spin direction through the 180° Ni^{2+}-O-Sn exchange interaction (3.6 T per Ni ion) [46]. The Ni-O distances in $NiTiO_3$, NiO, and $Ni_{5.15}Sn_{0.85}(O_2BO_3)_2$ are essentially the same (2.090, 2.089. and 2.087 Å, respectively); hence the transfer and overlap parameters can be assumed to be close. Moreover, spin polarization of Sn is mainly caused by 180° indirect exchange coupling through the oxygen anions involving the half-filled e_g orbitals [45–49]. The transferred hyperfine field of 19.4 T observed in $Ni_{5.15}Sn_{0.85}(O_2BO_3)_2$, which is comparable with that found in NiO, suggests that the Sn ions which feel such a large field are located at the 2-3 layer, where they have four superexchange bonds at 162° and the strongest direct exchange interactions due to the shortest intermetallic distance Sn-Ni ($d_{(2\text{-}3)} = 2.71$ Å). The Sn ions in other sites involve only

90° and 120° superexchange bonds and larger intermetallic distances; see Table III. Even in a hypothetical ferromagnetic structure for the Ni ions, they would not be able to create such a large field at the Sn nuclei. So, the 37% of the Sn ions at the 2-3 layer feel a transferred hyperfine field. This is in fair agreement with XRD experiments that show that 31% of the Sn ions are located in the 2-3 layers.

Important information about the magnetic structure can be obtained from the angle θ between the main component of the electric field gradient V_{ZZ} axis and the direction of the hyperfine field. In $NiTiO_3$ [45] and more recently in $Co_5SnB_2O_{10}$ [18] asymmetric magnetic spectra allow us to determine the direction of the spin as well as the sign of V_{ZZ} unambiguously. In $Ni_{5.15}Sn_{0.85}(O_2BO_3)_2$ the symmetric spectra lead to $\theta = 55°$, and several interpretations are possible. A symmetric spectrum means a quadrupole splitting equal to zero, and in this case any angle is possible. However a structural transition responsible for such a drastic reduction of the quadrupole splitting is very improbable. A second possibility is that the angle between V_{ZZ} and B_{hf} may be exactly 55°, which could imply a well ordered magnetic structure (the spin polarization of the spin transferred to the Sn nuclei should coincide in direction with the moment of the Ni). A third possibility is that all angles in the range $0 \leqslant \theta \leqslant 90°$ occur with equal probability, and this is related to a not well defined magnetic structure or spin glass state. This third option is more likely due to the disorder produced by the nonmagnetic Sn ions and the different paths of magnetic interactions, involving direct exchange (with strong *d*-*d* overlap) and superexchange. Even double exchange could be present.

The crystal structure of the subsystem formed by the 2-3 layers and Ni ions at site 5 has almost the same structure of the subsystem formed by the three-leg ladders (formed by the 4-2-4 sites) and the Ni ions at site 3 of the ludwigite $Ni_5GeB_2O_{10}$. Their crystallographic parameters, Ni-Ni and Ni-O lengths, and Ni-O-Ni bond angles are essentially the same [10]. In $Ni_5GeB_2O_{10}$ the competition between antiferromagnetic and ferromagnetic superexchange interactions, weakened by the presence of the nonmagnetic Ge ions, seems to give rise to magnetic frustration, and a partial ordering or spin glass state is established [10]. Assuming that the nonmagnetic Sn ions play the same role that the Ge in these samples, the substructure formed by the 2-3 layer and Ni at site 5 in $Ni_{5.15}Sn_{0.85}(O_2BO_3)_2$ is expected to have the same magnetic behavior as the $Ni_5GeB_2O_{10}$. Thus, below 180 K a partial magnetic order, spin freezing, or a spin glass state for this subsystem is in full agreement with the third interpretation given for the analysis of the Mössbauer magnetic subspectrum. This is also consistent with the observed shift of the position of the peak in the susceptibility with increasing frequency. Besides, this is further supported by the fact that this magnetic transition does not show up in the macroscopic specific heat measurements. So, it is very reasonable to attribute the magnetic transition observed at 180 K to a partial ordering or spin glass of the 2-3 layer. However, we cannot distinguish if the freezing is associated with single spins or with rather large clusters of parallel oriented spins.

XRD experiments did not show the presence of Sn at site 5. In the hypothetical case that a very small fraction is present, they should also feel a transferred hyperfine field because the magnetic interactions in the subsystem formed by sites 2, 3, and 5 are strong. It is possible that the presence of Sn atoms at site 5 would already be included in the magnetic subspectrum. Thus the remaining 63% Sn ions, that do not feel a measurable hyperfine magnetic field, are at the 1-4 layer as indicated by XRD. The absence of a hyperfine magnetic field at the Sn nuclei means that if a spin structure is established in the 1-4 layer it should have an arrangement such that the transferred hyperfine field at the Sn nuclei is completely compensated. Since the Sn ions are randomly distributed at site 1 (see Fig. 10), a spin arrangement with those specific characteristics is very unlikely. Paramagnetic spectra due to the presence of small nanoparticles with superparamagnetic relaxation are ruled out since we are dealing with rather large dimension single crystals. On the other hand, fluctuations of the Ni spin direction could give rise to fluctuating supertransferred magnetic field at the Sn nuclei and if its relaxation time τ is much lower than the Larmor precession time τ_L (of the nuclear spin of the ^{119}Sn) the hyperfine field seen by the Sn nuclei (the time average of this fluctuating field) will be zero and a paramagnetic spectra will be observed, as is the case in the low-temperature Mössbauer spectra of the $Ni_{5.15}Sn_{0.85}(O_2BO_3)_2$.

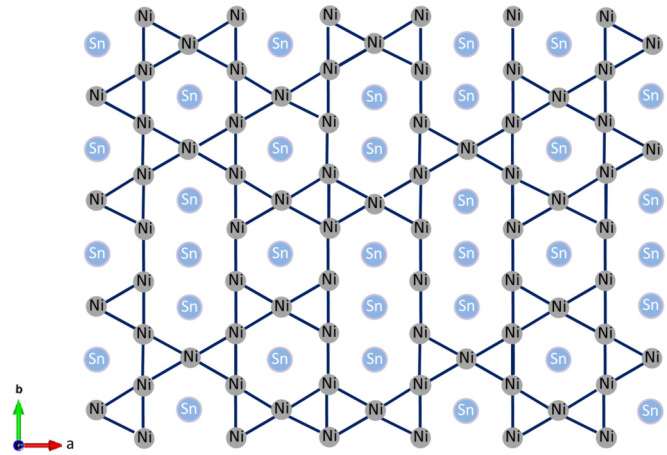

FIG. 10. Magnetic interactions of the Ni ions (black lines) in the 1-4 layer, considering randomly distributed nonmagnetic Sn ions on site 1 (blue circles).

In the 1-4 layer the magnetic ions are arranged in a two-dimensional triangular lattice, which is associated with geometric frustration in the case of AFM interactions between magnetic ions. The presence of nonmagnetic Sn ions at site 1 produces site occupancy disorder, but does not destroy the triangular configuration of the Ni atoms, as can be seen in Fig. 10. Moreover, most of the magnetic ions are coordinated with four magnetic ions instead of six, as in a Kagomé lattice, increasing geometric frustration [50]. Thus, considering structural features, magnetic frustration is highly expected in 1-4 layer and is consistent with the Mössbauer results that indicate a fast fluctuation of the Ni spin directions.

More difficult to explain is the peak observed at 20 K in the specific heat measurements, since no corresponding visible changes are observed at the same temperature in the magnetization measurements. However, the Mössbauer spectroscopy can help us in its interpretation. The line broadening, corresponding to the doublet of the Sn in the 1-4 layer, is

attributed to an unresolved hyperfine field at the Sn nuclei due to a supertransferred hyperfine interaction between the Sn nuclei and the surrounding Ni ions. The doublet below 180 K is assumed to be in a situation where the Ni ionic relaxation time is comparable with the Larmor precession time of the Sn nuclei. Below ∼100 K, a sharp increase of the linewidth is observed, indicating an increase of the relaxation time, i.e., a decrease of the magnetic fluctuation. Other frustrated systems with two-dimensional triangular or Kagomé lattices show a specific heat peak related to a saturation of the spin fluctuation rate [21,51]. The frustrated Kagomé lattice spin system $SrCr_8Ga_4O_{19}$ [52] exhibits a field-independent specific heat with a peak at ∼3.5 K and a small cusp in the susceptibility data. Below this temperature, a saturation of the spin fluctuation rate was observed, but spin fluctuation persists down to 100 mK. No spin freezing was observed for this compound. On the other hand, in $NiGa_2S_4$, a two-dimensional Heisenberg triangular-lattice antiferromagnet, the specific heat displays a peak at ∼10 K, whose position and amplitude are independent of applied magnetic fields (at least, up to 7 T) and the susceptibility shows a broad maximum at the same temperature [21]. Muon spin rotation and relaxation (μSR) results have demonstrated that there is a slowing down of magnetic fluctuations as this compound is cooled down through T_C rather than a spin freezing [53]. Recent μSR and susceptibility data show a well-defined 2D phase transition at $T_f = 8.5$ K (leading to a disordered AFM ground state) below which the $NiGa_2S_4$ is neither a conventional magnet nor a singlet spin liquid [54]. Several scenarios have been proposed to describe the experimental results; however, no theory so far is able to fully account for the unusual magnetism of this compound [53–55].

At low temperatures (<5 K), the linear dependence of the specific heat with temperature was a new and unexpected result in oxyborates. This linear T dependence of the specific heat at low temperatures is unusual for a magnetic insulator having a 2D frustrated lattice. However, a linear dependence has been found in the 6H-B phase of $Ba_3NiSb_2O_9$ with a Ni^{2+} triangular lattice [19,20] and is a common feature among QSL candidates [56–58]. Thus, the linear T dependence of the specific heat found in hulsite $Ni_{5.15}Sn_{0.85}(O_2BO_3)_2$ in zero-field protocol suggests a spin liquid behavior of the 1-4 layer. Evidently, a linear contribution with T due to local disorder in the 2-3 layer could also be included, but its contribution should not be dominant. The application of a sufficiently strong magnetic field could reinforce ferromagnetic correlations, eventually in the two types of layers, and give rise to ferromagnetic magnon excitations.

The specific heat, ac susceptibility and Mössbauer results in hulsite $Ni_{5.15}Sn_{0.85}(O_2BO_3)_2$ are consistent with the assumption that magnetic fluctuations of the Ni spins occurs in the 1-4 layer, which has a triangular lattice. The absence of magnetic ordering in this Ni layer could be related to the magnetic frustration originated by the triangular arrangement of the magnetic Ni ions with antiferromagnetic interactions.

IV. CONCLUSION

Combining macroscopic and local experimental techniques, our results demonstrate that the magnetic and thermodynamic behavior of $Ni_{5.15}Sn_{0.85}(O_2BO_3)_2$ can be understood in terms of two independent magnetic subsystems. At 180 K, the first subsystem formed by 2-3 layers, where strong d-d overlap is expected, orders magnetically in a spin-glass-like state. Mössbauer spectroscopy gives evidence for local disorder in this layer. In addition, Mössbauer spectroscopy shows that Ni atoms at the 1-4 layer do not *feel* a measurable transferred magnetic hyperfine field, indicating that this layer does not order magnetically down to 3 K. However, a decrease of the magnetic fluctuations is observed at low temperatures. Thus, this is a compound with a complex magnetic structure, where magnetic ordering in the form of a spin-glass-like state coexists with magnetic fluctuations at low temperatures. Further measurements need to be done to clarify the nature of these distinct magnetic behaviors.

ACKNOWLEDGMENTS

LNLS is acknowledged for concession of beam time. We also acknowledge LDRX-UFF (Universidade Federal Fluminense, Brazil) for use of their laboratory facilities. Support from the Brazilian agencies CNPq, FAPERJ, and FAPES is gratefully acknowledged.

[1] J. P. Attfield, J. F. Clarke, and D. A. Perkins, Physica B (Amsterdam) **180**, 581 (1992).

[2] R. B. Guimaraes, M. Mir, J. C. Fernandes, M. A. Continentino, H. A. Borges, G. Cernicchiaro, M. B. Fontes, D. R. S. Candela, and E. Baggio-Saitovich, Phys. Rev. B **60**, 6617 (1999).

[3] J. Bartolome, A. Arauzo, N. V. Kazak, N. B. Ivanova, S. G. Ovchinnikov, Y. V. Knyazev, and I. S. Lyubutin, Phys. Rev. B **83**, 144426 (2011).

[4] M. Angst, R. P. Hermann, W. Schweika, J.-W. Kim, P. Khalifah, H. J. Xiang, M.-H. Whangbo, D.-H. Kim, B. C. Sales, and D. Mandrus, Phys. Rev. Lett. **99**, 256402 (2007).

[5] D. C. Freitas, C. P. C. Medrano, D. R. Sanchez, M. N. Regueiro, J. A. Rodriguez-Velamazan, and M. A. Continentino, Phys. Rev. B **94**, 174409 (2016).

[6] N. Kazak, M. Platunov, Y. V. Knyazev, N. Ivanova, O. Bayukov, A. Vasiliev, L. Bezmaternykh, V. Nizhankovskii, S. Y. Gavrilkin, K. Lamonova *et al.*, J. Magn. Magn. Mater. **393**, 316 (2015).

[7] N. Ivanova, N. Kazak, Y. V. Knyazev, D. Velikanov, L. Bezmaternykh, S. Ovchinnikov, A. Vasiliev, M. Platunov, J. Bartolomé, and G. Patrin, J. Exp. Theor. Phys. **113**, 1015 (2011).

[8] D. C. Freitas, M. A. Continentino, R. B. Guimaraes, J. C. Fernandes, E. P. Oliveira, R. E. Santelli, J. Ellena, G. G. Eslava, and L. Ghivelder, Phys. Rev. B **79**, 134437 (2009).

[9] D. C. Freitas, R. B. Guimaraes, D. R. Sanchez, J. C. Fernandes, M. A. Continentino, J. Ellena, A. Kitada, H. Kageyama, A. Matsuo, K. Kindo *et al.*, Phys. Rev. B **81**, 024432 (2010).

[10] S. Sofronova, L. Bezmaternykh, E. Eremin, I. Nazarenko, N. Volkov, A. Kartashev, and E. Moshkina, J. Magn. Magn. Mater. **401**, 217 (2016).

[11] A. Arauzo, N. V. Kazak, N. B. Ivanova, M. S. Platunov, Y. V. Knyazev, O. A. Bayukov, L. N. Bezmaternykh, I. S. Lyubutin, K. V. Frolov, S. G. Ovchinnikov *et al.*, J. Magn. Magn. Mater. **392**, 114 (2015).

[12] I. Lyubutin, N. Y. Korotkov, K. Frolov, N. Kazak, M. Platunov, Y. V. Knyazev, L. Bezmaternykh, S. Ovchinnikov, A. Arauzo, and J. Bartolomé, J. Alloys Compd. **642**, 204 (2015).

[13] T. G. Rappoport, L. Ghivelder, J. C. Fernandes, R. B. Guimarães, and M. A. Continentino, Phys. Rev. B **75**, 054422 (2007).

[14] K. Bluhm, H. Müller-Buschbaum, and L. Walz, J. Less-Common Met. **158**, 339 (1990).

[15] D. C. Freitas, R. B. Guimarães, J. C. Fernandes, M. A. Continentino, C. B. Pinheiro, J. A. L. C. Resende, G. G. Eslava, and L. Ghivelder, Phys. Rev. B **81**, 174403 (2010).

[16] J. Larrea J., D. R. Sánchez, F. J. Litterst, E. M. Baggio-Saitovitch, J. C. Fernandes, R. B. Guimarães, and M. A. Continentino, Phys. Rev. B **70**, 174452 (2004).

[17] R. B. Guimaraes, J. C. Fernandes, M. A. Continentino, H. A. Borges, C. S. Moura, J. B. M. da Cunha, and C. A. dos Santos, Phys. Rev. B **56**, 292 (1997).

[18] C. P. C. Medrano, D. C. Freitas, D. R. Sanchez, C. B. Pinheiro, G. G. Eslava, L. Ghivelder, and M. A. Continentino, Phys. Rev. B **91**, 054402 (2015).

[19] J. G. Cheng, G. Li, L. Balicas, J. S. Zhou, J. B. Goodenough, C. Xu, and H. D. Zhou, Phys. Rev. Lett. **107**, 197204 (2011).

[20] B. Fåk, S. Bieri, E. Canévet, L. Messio, C. Payen, M. Viaud, C. Guillot-Deudon, C. Darie, J. Ollivier, and P. Mendels, Phys. Rev. B **95**, 060402 (2017).

[21] S. Nakatsuji, Y. Nambu, H. Tonomura, O. Sakai, S. Jonas, C. Broholm, H. Tsunetsugu, Y. Qiu, and Y. Maeno, Science **309**, 1697 (2005).

[22] O. Mustonen, S. Vasala, E. Sadrollahi, K. Schmidt, C. Baines, H. Walker, I. Terasaki, F. Litterst, E. Baggio-Saitovitch, and M. Karppinen, Nat. Commun. **9**, 1085 (2018).

[23] Apex3 code, Bruker AXS Inc., Madison, Wisconsin, 2012.

[24] G. M. Sheldrick, CELL_NOW code, University of Göttingen, 2008.

[25] Saint code, Bruker AXS Inc., Madison, Wisconsin, 1999.

[26] G. M. Sheldrick, Twinabs, Program for Empirical Absorption Correction of Area Detector Data, University of Göttingen, 1996.

[27] G. M. Sheldrick, Acta Crystallogr. Sect. C **71**, 3 (2015).

[28] L. J. Farrugia, J. Appl. Crystallogr. **45**, 849 (2012).

[29] C. B. Hübschle, G. M. Sheldrick, and B. Dittrich, J. Appl. Crystallogr. **44**, 1281 (2011).

[30] P. Paufler, Acta Crystallogr. Sect. A **60**, 641 (2004).

[31] B. Ravel and M. Newville, J. Synchrotron Radiat. **12**, 537 (2005).

[32] T. Jiang and D. Ellis, J. Mater. Res. **11**, 2242 (1996).

[33] L. Galoisy and G. Calas, Geochim. Cosmochim. Acta **57**, 3613 (1993).

[34] J. McBreen, W. O'Grady, G. Tourillon, E. Dartyge, A. Fontaine, and K. Pandya, J. Phys. Chem. **93**, 6308 (1989).

[35] L. Galoisy and G. Calas, Mater. Res. Bull. **28**, 221 (1993).

[36] R. Cairns and E. Ott, J. Am. Chem. Soc. **56**, 1094 (1934).

[37] M. Lenglet, R. Guillamet, J. Dürr, D. Gryffroy, and R. Vandenberghe, Solid State Commun. **74**, 1035 (1990).

[38] A. Mansour, C. Melendres, M. Pankuch, and R. Brizzolara, J. Electrochem. Soc. **141**, L69 (1994).

[39] L. Coutrim, E. Bittar, F. Stavale, F. Garcia, E. Baggio-Saitovitch, M. Abbate, R. Mossanek, H. Martins, D. Tobia, P. Pagliuso *et al.*, Phys. Rev. B **93**, 174406 (2016).

[40] C. P. C. Medrano, D. C. Freitas, E. C. Passamani, C. B. Pinheiro, E. Baggio-Saitovitch, M. A. Continentino, and D. R. Sanchez, Phys. Rev. B **95**, 214419 (2017).

[41] K. Fischer and J. Hertz, *Spin Glasses*, Cambridge Studies in Magnetism (Cambridge University Press, Cambridge, 1993).

[42] N. Greenwood and T. Gibb, *Mössbauer Spectroscopy* (Chapman and Hall, London, 1971).

[43] I. Lyubutin, T. Dmitrieva, and A. Stepin, J. Exp. Theor. Phys. **88**, 590 (1999).

[44] K. Motida and S. Miyahara, J. Phys. Soc. Jpn. **28**, 1188 (1970).

[45] P. Fabritchnyi, A. Wattiaux, M. Korolenko, M. Afanasov, and C. Delmas, Solid State Commun. **149**, 1535 (2009).

[46] V. Tkachenko, M. Korolenko, M. Danot, and P. Fabrichnyi, Russ. J. Inorg. Chem. **50**, 1247 (2005).

[47] P. B. Fabrichnyi, E. V. Lamykin, A. M. Babeshkin, and Nesmeyanov, Fiz. Tverd. Tela **13**, 3417 (1971).

[48] M. Korolenko, S. Medvedev, V. Tkachenko, M. Afanasov, M. Danot, and P. Fabrichnyi, Russ. J. Inorg. Chem. **49**, 603 (2004).

[49] P. Fabrichnyi, M. Korolenko, V. Tkachenko, M. Danot, and C. Payen, Russ. J. Inorg. Chem. **52**, 1262 (2007).

[50] L. Balents, Nature (London) **464**, 199 (2010).

[51] Y. Uemura, A. Keren, K. Kojima, L. Le, G. Luke, W. Wu, Y. Ajiro, T. Asano, Y. Kuriyama, M. Mekata *et al.*, Phys. Rev. Lett. **73**, 3306 (1994).

[52] A. P. Ramirez, B. Hessen, and M. Winklemann, Phys. Rev. Lett. **84**, 2957 (2000).

[53] Y. Nambu, J. S. Gardner, D. E. MacLaughlin, C. Stock, H. Endo, S. Jonas, T. J. Sato, S. Nakatsuji, and C. Broholm, Phys. Rev. Lett. **115**, 127202 (2015).

[54] D. E. MacLaughlin, Y. Nambu, S. Nakatsuji, R. H. Heffner, L. Shu, O. O. Bernal, and K. Ishida, Phys. Rev. B **78**, 220403 (2008).

[55] A. Yaouanc, P. D. Dalmas de Réotier, Y. Chapuis, C. Marin, G. Lapertot, A. Cervellino, and A. Amato, Phys. Rev. B **77**, 092403 (2008).

[56] S. Yamashita, Y. Nakazawa, M. Oguni, Y. Oshima, H. Nojiri, Y. Shimizu, K. Miyagawa, and K. Kanoda, Nat. Phys. **4**, 459 (2008).

[57] S. Yamashita, T. Yamamoto, Y. Nakazawa, M. Tamura, and R. Kato, Nat. Commun. **2**, 275 (2011).

[58] H. D. Zhou, E. S. Choi, G. Li, L. Balicas, C. R. Wiebe, Y. Qiu, J. R. D. Copley, and J. S. Gardner, Phys. Rev. Lett. **106**, 147204 (2011).